JACS
JOURNAL OF THE AMERICAN CHEMICAL SOCIETY

ARTICLE

pubs.acs.org/JACS

Dynamics of Lysine Side-Chain Amino Groups in a Protein Studied by Heteronuclear $^{1}H-^{15}N$ NMR Spectroscopy

Alexandre Esadze,[†] Da-Wei Li,[‡] Tianzhi Wang,[†] Rafael Brüschweiler,[‡] and Junji Iwahara*[,†]

[†]Department of Biochemistry and Molecular Biology, Sealy Center for Structural Biology and Molecular Biophysics, University of Texas Medical Branch, Galveston, Texas 77555, United States

[‡]Chemical Sciences Laboratory, Department of Chemistry and Biochemistry, and National High Magnetic Field Laboratory, Florida State University, Tallahassee, Florida 32306, United States

Supporting Information

ABSTRACT: Despite their importance in macromolecular interactions and functions, the dynamics of lysine side-chain amino groups in proteins are not well understood. In this study, we have developed the methodology for the investigations of the dynamics of lysine NH_3^+ groups by NMR spectroscopy and computation. By using $^{1}H-^{15}N$ heteronuclear correlation experiments optimized for $^{15}NH_3^+$ moieties, we have analyzed the dynamic behavior of individual lysine NH_3^+ groups in human ubiquitin at 2 °C and pH 5. We modified the theoretical framework developed previously for CH_3 groups and used it to analyze ^{15}N relaxation data for the NH_3^+ groups. For six lysine NH_3^+ groups out of seven in ubiquitin, we have determined model-free order parameters, correlation times for bond rotation, and reorientation of the symmetry axis occurring on a pico- to nanosecond time scale. From CPMG relaxation dispersion experiment for lysine NH_3^+ groups, slower dynamics occurring on a millisecond time scale have also been detected for Lys27. The NH_3^+ groups of Lys48, which plays a key role as the linkage site in ubiquitination for proteasomal degradation, was found to be highly mobile with the lowest order parameter among the six NH_3^+ groups analyzed by NMR. We compared the experimental order parameters for the lysine NH_3^+ groups with those from a 1 μs molecular dynamics simulation in explicit solvent and found good agreement between the two. Furthermore, both the computer simulation and the experimental correlation times for the bond rotations of NH_3^+ groups suggest that their hydrogen bonding is highly dynamic with a subnanosecond lifetime. This study demonstrates the utility of combining NMR experiment and simulation for an in-depth characterization of the dynamics of these functionally most important side-chains of ubiquitin.

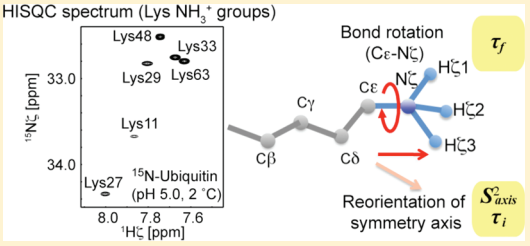

INTRODUCTION

The side-chain amino groups of lysine residues in proteins play an important role in many processes involving macromolecular interactions and reactions. With a typical pK_a around 10.5, the lysine amino groups in proteins are predominantly protonated in the form of NH_3^+ at neutral and acidic pH. They can form salt bridges with acidic groups in proteins and nucleic acids and thereby significantly contribute to protein stability and to both the strength and the specificity of intermolecular interactions. Despite their importance, very little is known about the dynamics of NH_3^+ groups in proteins because of a lack of suitable tools for their experimental investigations.

For NMR studies of lysine NH_3^+, a major challenge is their rapid hydrogen exchange with water. Hydrogen exchange rates for lysine amino groups typically exceed 1000 s^{-1} at a physiological pH and temperature, making the direct ^{1}H NMR detection of lysine NH_3^+ groups in proteins hard.[1,2] However, three factors can make the hydrogen exchange rate for a lysine side-chain less than 100 s^{-1}, permitting direct ^{1}H detection: (1) structural effects (e.g., steric hindrance and hydrogen bonds) that make the hydrogen exchange slower,[3−5] (2) low pH, and (3) low temperature. In general, a reduction of pH by one unit reduces the hydrogen exchange rate by a factor of 10.[1,6] With an activation energy for the hydrogen exchange around ∼9 kcal/mol, hydrogen exchange for a lysine NH_3^+ group at 2 °C occurs roughly 20-fold more slowly than at 32 °C.[2] Even though the hydrogen exchange is slow enough for the direct ^{1}H detection of the NH_3^+ groups, the hydrogen exchange can adversely affect the spectral behavior along the ^{15}N dimension in normal $^{1}H-^{15}N$ heteronuclear correlation experiments such as HSQC[7] and HMQC.[8,9] Recently, it was demonstrated that scalar relaxation due to the hydrogen exchange can make the ^{15}N lineshapes of NH_3^+ groups substantially broader than those of backbone amide in HSQC and HMQC spectra, despite the fact that the intrinsic ^{15}N transverse relaxation for NH_3^+ groups is much slower than that of backbone amide groups.[3] To address this problem, Iwahara et al. developed the HISQC pulse sequence in which the effects of scalar relaxation in the ^{15}N-evolution period

Received: August 31, 2010
Published: December 27, 2010

are eliminated.[3] As compared to the HSQC and HMQC experiments, the HISQC experiment dramatically improves ^{15}N lineshapes and signal intensities for lysine side-chain NH_3^+ groups.[3] This is in contrast to the case of $^{13}CH_3$ groups in proteins, for which HMQC (methyl-TROSY) provides the highest sensitivity.[10,11] The HISQC experiment has been applied to lysine side-chain amino groups in various environments.[3,5,12−14]

In this work, we have extended the application of the ^{1}H−^{15}N heteronuclear NMR spectroscopy to the analysis of the conformational dynamics of NH_3^+ groups using human ubiquitin as a model system. Investigation of the dynamics of lysine side-chains for this model system is particularly relevant because the lysine NH_3^+ groups play crucial roles in the various functions performed by ubiquitin. The dynamics of the lysine NH_3^+ groups were analyzed using ^{15}N relaxation parameters measured with the HISQC-based pulse sequences. Using the theoretical framework originally developed for $^{13}CH_3$ groups, we report the quantitative dynamics characterization of Lys NH_3^+ side-chain groups in terms of model-free order parameters and associated correlation times.

THEORETICAL CONSIDERATIONS

Effects of Rapid Hydrogen Exchange on Heteronuclear NMR of NH_3^+ Groups. The presence of hydrogen exchange with surrounding water, which is one of the major differences between CH_3 and NH_3^+ systems, causes rapid scalar relaxation[15] of transverse magnetization that is antiphase with respect to ^{1}H. Hydrogen exchange occurring with a pseudofirst-order rate constant k_{ex}^{water} enhances relaxation of the $2N_+H_z$, $4N_+H_zH_z$, and $8N_+H_zH_zH_z$ terms by k_{ex}^{water}, $2k_{ex}^{water}$, and $3k_{ex}^{water}$, respectively.[3] Hydrogen exchange also enhances relaxation of longitudinal multispin orders such as $2N_zH_z$, $4N_zH_zH_z$, and $8N_zH_zH_z$ in the same fashion. Because $k_{ex}^{water} > 20\ s^{-1}$ is typical for NH_3^+ groups even if the hydrogen exchange is slow enough for direct observation of the protons, scalar relaxation due to hydrogen exchange makes the relaxation of most ^{15}N product operator terms (except N_x, N_y, and N_z) much faster than the "intrinsic" ^{15}N relaxation due to dipolar and CSA interactions. For this reason, most NMR techniques available for determination of order parameters of CH_3 groups (e.g., reviewed in ref 16) cannot be directly applied to NH_3^+ groups. Use of the $^{15}NHD_2^+$ (or $^{15}NH_2D^+$) isotopomers for the dynamic investigations is impractical because the rapid hydrogen exchange can convert them during the period for relaxation into different isotopomers, which makes the analysis difficult (note that the properties of different isotopomers differ in terms of both relaxation and chemical shifts). Thus, we measure the intrinsic ^{15}N relaxation of $^{15}NH_3^+$ groups in the absence of D_2O, while a deuterium signal from a separated compartment is used as NMR lock (see below).

In the design of heteronuclear NMR experiments for NH_3^+ groups, it is critical to maintain in-phase single quantum coherence N_+ ($=N_x + iN_y$) throughout the ^{15}N evolution period.[3] Use of a single ^{1}H 180° pulse for the decoupling in the evolution period results in a very broad line-width of the ^{15}N resonances of NH_3^+ groups because during the half periods before and after the 180° pulse, antiphase terms $2N_+H_z$, $4N_+H_zH_z$, and $8N_+H_zH_zH_z$ are generated, which decay very quickly due to the hydrogen exchange. In the pulse sequences used in this work, the in-phase single quantum term N_+ is maintained throughout the t_1 period in the same way as in the HISQC experiment, which permits observation of NH_3^+ signals with very narrow ^{15}N lineshapes and high sensitivity.

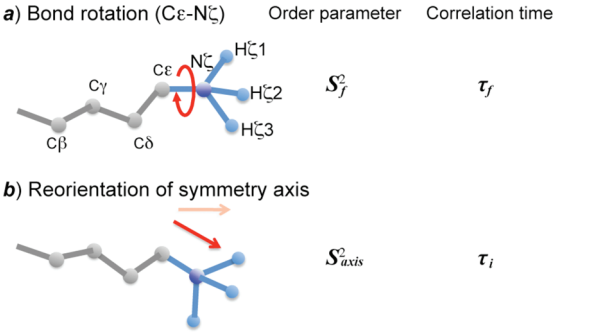

Figure 1. Model for internal motions of lysine NH_3^+ groups in proteins. Assuming that the bond rotation (a) and reorientation of the symmetry axis (b) are not coupled, the spectral density function represented by eq 1 is derived from the product of correlation functions of overall motions, bond rotation, and reorientation of symmetry axis. Assuming ideal geometry for NH_3^+ groups,[18] $S^2_f = 0.111$ for $J_{auto}(\omega)$ and $J_{NHNH}(\omega)$ and $S^2_f = 0.167$ for $J_{HHHN}(\omega)$ were used in the present study. S^2_{axis}, τ_f, and τ_i were determined from the NMR data.

Lysine NH_3^+ Groups as AX_3 Spin Systems. Because both ^{15}N−$^1H_3$ and ^{13}C−$^1H_3$ groups represent AX_3 spin systems, the theoretical framework established for ^{13}C relaxation of methyl groups in macromolecules can be directly adopted for ^{15}N relaxation of the ^{15}N−$^1H_3^+$ groups due to the following characteristics: (1) ^{15}N chemical shift anisotropy (CSA) defined as $|\sigma_\parallel - \sigma_\perp|$ is as small as 15 ppm for lysine NH_3^+ groups,[17] which renders CSA relaxation (as well as CSA-related cross-correlated relaxation) negligible; and (2) the covalent geometry for an NH_3^+ group is almost ideally tetrahedral even if it forms a salt-bridge with an acidic group.[18] Judging from the previous NMR studies on $^{15}NH_3^+$ groups of small compounds,[19] the spin-rotation mechanism[20] is also negligible for the NH_3^+ groups in macromolecules at a high magnetic field. Thus, the dipole−dipole (DD) relaxation terms and their cross correlations govern the ^{15}N relaxation of lysine NH_3^+ groups. For the DD autorelaxation and DD/DD cross correlation, a general form of the spectral density function for pairs of interacting spins ij and kl in an AX_3 spin system in a macromolecule is given by:[21]

$$J_{ijkl}(\omega) = \frac{1}{4\pi}\zeta_{ij}\zeta_{kl}\left[\frac{S^2_{f,(ij,kl)}S^2_{axis}\tau_m}{1+\omega^2\tau_m^2} + \frac{S^2_{axis}\{P_2(\cos\chi_{ij,kl}) - S^2_{f,(ij,kl)}\}\tau_1}{1+\omega^2\tau_1^2} + \frac{S^2_{f,(ij,kl)}(1-S^2_{axis})\tau_2}{1+\omega^2\tau_2^2} + \frac{(1-S^2_{axis})\{P_2(\cos\chi_{ij,kl}) - S^2_{f,(ij,kl)}\}\tau_3}{1+\omega^2\tau_3^2}\right] \quad (1)$$

where $\zeta_{ij} = (6\pi/5)^{1/2}(\mu_0/4\pi)(h/2\pi)\gamma_i\gamma_j r_{ij}^{-3}$; μ_0 is the vacuum permeability; h is the Planck constant; γ is a nuclear gyromagnetic ratio; r_{ij} is the distance between spins i and j; $\chi_{ij,kl}$ is the angle between the ij and kl vectors; S^2_{axis} is a generalized order parameter[22] for the symmetry axis of the AX_3 spin system; $S^2_{f,(ij,kl)}$ is an order parameter for bond rotation around the symmetry axis; $P_2(x) = (3x^2 - 1)/2$; τ_m is the overall molecular rotational correlation time; $\tau_1^{-1} = \tau_m^{-1} + \tau_f^{-1}$; $\tau_2^{-1} = \tau_m^{-1} + \tau_i^{-1}$; $\tau_3^{-1} = \tau_m^{-1} + \tau_f^{-1} + \tau_i^{-1}$; τ_i is a correlation time for reorientation of the symmetry axis; and τ_f is a correlation time for bond rotation around the symmetry axis. The motional model for a lysine NH_3^+ group is depicted in Figure 1. For autorelaxation, $i = k =$ N and $j = l =$ H, and the corresponding spectral density is denoted by $J_{auto}(\omega)$. For N−H/N−H cross correlation, the corresponding spectral density is denoted by $J_{NHNH}(\omega)$, for which $i = k =$ N, but

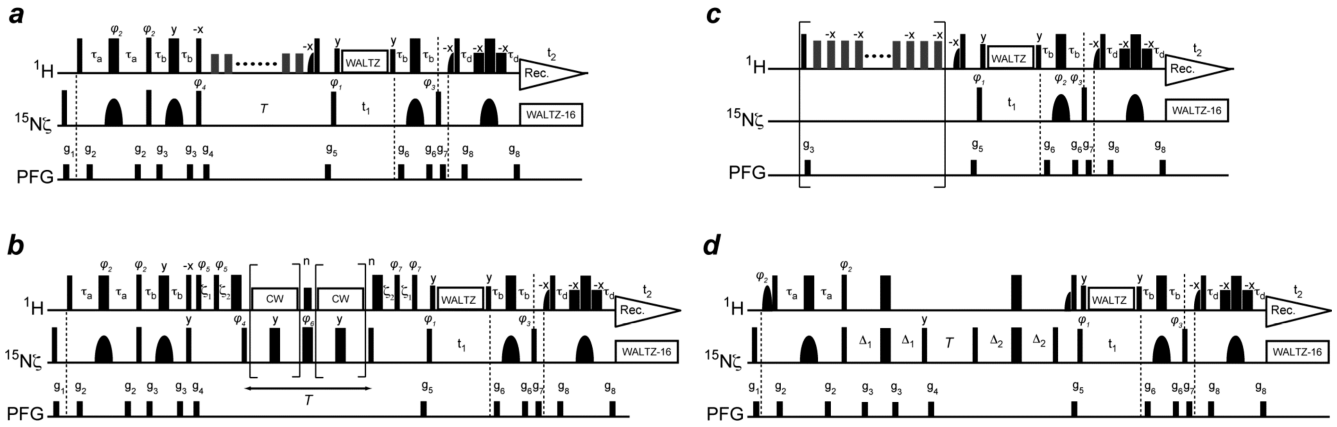

Figure 2. Pulse sequences for the ^{15}N relaxation measurement for lysine side-chain NH_3^+ groups. Thin and bold bars in black represent hard rectangular 90° and 180° pulses, respectively. Water-selective half-Gaussian (2.1 ms) and soft-rectangular (1.2 ms) 90° pulses are represented by half-bell and short-bold shapes, respectively. Unless indicated otherwise, pulse phases are along x, and the carrier position for ^{1}H was set to the position of the water resonance. The rf strengths for hard rectangular ^{1}H and ^{15}N pulses were 40 and 6.6 kHz, respectively. The rf strengths of ^{1}H WALTZ-16 composite decoupling[83] during the ^{15}N evolution period were 4.5 and 3.5 kHz for the 800 and 600 MHz spectrometers, respectively. ^{15}N carrier position was set to 33.1 ppm. ^{15}N-decouling during the t_2 detection period was performed with WALTZ-16 (rf strength, 1.0 kHz). A gray bell-shape for ^{15}N represents an r-SNOB[84] 180° pulse (1.03 ms) for inversion and refocusing. The delays τ_a and τ_b were 2.7 and 2.0 ms, respectively. Quadrature detection in the t_1 domain was achieved using States-TPPI, incrementing the phase φ_1. Pulsed field gradients were optimized to minimize the water signal. The water flip back principle[38,85] is implemented in all pulse sequences shown in this figure. (a) ^{15}N R_1 measurement. Although it is not essential due to negligible CSA-DD cross correlation for NH_3^+, a ^{1}H 180° pulse (null at water resonance) was applied every 10 ms during the delay T for longitudinal relaxation. Phase cycles: $\varphi_1 = (2y, 2(-y))$, $\varphi_2 = (y, -y)$, $\varphi_3 = (4x, 4(-x))$, $\varphi_4 = (8y, 8(-y))$, and receiver = $(x, -x, -x, x, 2(-x, x, x, -x), x, -x, x)$. The ^{15}N R_1 rates were obtained via fitting with $I(T) = I(0)\exp(-R_1T)$. (b) ^{15}N $R_{2,\mathrm{ini}}$ measurement. The rf strength for ^{15}N pulses for the CPMG scheme was 5.4 kHz. ^{1}H carrier position was shifted to 7.8 ppm right after the gradient g4 and set back to the position of water resonance right after the gradient g5. The rf strength $\omega_{CW}/2\pi$ of ^{1}H CW during the CPMG was set to 4.3 kHz, which was adjusted to satisfy $\omega_{CW}/2\pi = 2k\nu_{CPMG}$ (k, integer).[31] The delays ξ_1 and ξ_2 are for alignment of ^{1}H magnetization and given by $\xi_1 = 1/\omega_{CW} - (4/\pi)\tau_{90H}$ and $\xi_2 = \tau_{90N} - (2/\pi)\tau_{90H}$,[31,86] in which τ_{90} represents a length of a relevant 90° pulse. Phase cycles: $\varphi_1 = (4y, 4(-y))$, $\varphi_2 = (8y, 8(-y))$, $\varphi_3 = x$, $\varphi_4 = (x, -x)$, $\varphi_5 = (2y, 2(-y))$, $\varphi_6 = (2x, 2(-x))$, $\varphi_7 = (2(-y), 2y)$, and receiver = $(x, -x, x, -x, 2(-x, x, -x, x), x, -x, x, -x)$. A relatively long recycle delay (2.7 s) was used for this experiment to avoid RF amplifier duty-cycle problems arising from relatively long ^{1}H−CW and ^{15}N-CPMG schemes. Because a high stability of the ^{1}H amplifier is important for a long ^{1}H−CW, the actual output of the ^{1}H channel was confirmed using an oscilloscope before the experiments. The initial rates for ^{15}N transverse relaxation ($R_{2,\mathrm{ini}}$) were obtained via fitting with $I(T) = I(0)\exp(-R_{2,\mathrm{ini}}T)$ using only an initial linear region of the decay. (c) Heteronuclear ^{1}H−^{15}N NOE measurement. Measurement with ^{1}H saturation (5 s) was performed with a train of 180°x and 180°$(-x)$ pulses (rf strength, 11 kHz) with an interval of 10 ms. ^{1}H carrier position was at 7.8 ppm during the ^{1}H saturation period. The reference spectrum was measured without the scheme in the bracket. The recycle delay (including the saturation period) was set to 12 s for a 600 MHz spectrometer (18 s for 800 MHz). Phase cycles: $\varphi_1 = (y, -y)$, $\varphi_2 = (4x, 4y, 4(-x), 4(-y))$, $\varphi_3 = (2x, 2(-x))$, and receiver = $(x, -x, -x, x, -x, x, x, -x)$. Taking ^{15}N R_1 into consideration, the heteronuclear NOE was calculated as $\{I_{sat} - I_{ref}\exp(-R_1T_{sat})\}/[I_{ref}\{1 - \exp(R_1T_{sat})\}]$, where T_{sat} is the length of the ^{1}H saturation period; and I_{sat} and I_{ref} represent signal intensities in spectra measured with and without ^{1}H saturation, respectively. (d) Measurement of $R(4N_zH_zH_z)$. The delay Δ_1 was set to 3.4 ms $[=(4J_{NH})^{-1}]$ so that all magnetizations become $4N_zH_zH_z$ at the beginning of the delay T. The delay Δ_2 was set to 2.3 ms for the $4N_yH_zH_z \rightarrow N_y$ transfer. The initial shaped ^{1}H pulse is a water-selective E-BURP pulse (7 ms). Phase cycles: $\varphi_1 = (2y, 2(-y))$, $\varphi_2 = (y, -y)$, $\varphi_3 = (4x, 4(-x))$, $\varphi_4 = (8y, 8(-y))$, and receiver = $(x, -x, -x, x, 2(-x, x, x, -x), x, -x, -x, x)$. The relaxation rates $R(4N_zH_zH_z)$ were obtained via fitting with $I(T) = I(0)\exp\{-R(4N_zH_zH_z)T\}$.

j and l are different H spins in the spin system. Likewise, the spectral density for H−H/H−N cross correlation is denoted by $J_{HHHN}(\omega)$, for which $i = j$ = H; k, another H in the AX_3 system; and l = N. $S^2_{f,(ij,kl)}$ is given by $P_2(\cos\beta_{ij})P_2(\cos\beta_{kl})$, where β_{ij} is the angle between the vector ij and the symmetry axis.[21] The spectral density model eq 1 is a modification of eq 15 of Kay and Torchia[21] and is derived from the product of correlation functions for overall motions, internal motions of symmetry axis, and bond rotation.[23] The total number of parameters involved is identical for these equations, and if $\tau_i \gg \tau_f$, the equations become the same. We use eq 1 because the inequality $\tau_i \gg \tau_f$ does not necessarily hold for NH_3^+ groups, for example, due to the possible presence of a hydrogen bond that may slow the bond rotation.

Effects of the rotational anisotropy on $^{15}NH_3^+$ relaxation can be taken into consideration based on Woessner's theory.[24−28] As is evident from eq 6 of Tjandra et al.,[27] the effects are relatively minor if the relevant order parameters are small. Because the overall order parameters ($S^2_{axis}S^2_f$) for lysine NH_3^+ groups satisfy $S^2_{axis}S^2_f \ll (1 - S^2_{axis}S^2_f)$, the rotational anisotropy renders only very minor effects on $^{15}NH_3^+$ relaxation. The effects for the NH_3^+ groups are virtually negligible in the present case of ubiquitin, which has a small diffusion anisotropy ($D_\parallel/D_\perp$) of 1.17.

^{15}N Longitudinal Relaxation for NH_3^+ Groups. Analogous to ^{13}C longitudinal relaxation rate R_1 for CH_3 groups in proteins,[21] the effect of the cross correlation between N−H dipole−dipole interactions on ^{15}N R_1 of NH_3^+ groups is negligible, and ^{15}N R_1 is given by:

$$R_1 = 3J_{auto}(\omega_N) + 6J_{auto}(\omega_H + \omega_N) + J_{auto}(\omega_H - \omega_N) \quad (2)$$

Figure 2a shows a pulse sequence to measure ^{15}N R_1 for lysine NH_3^+ groups. In this pulse sequence as well as the other three pulse sequences in Figure 2, the delay τ_b was chosen such that $3\cos^2(2\pi J_{NH}\tau_b) - 1 = 0$. In this way, the $2N_yH_z \rightarrow 4N_xH_zH_z$ transfer in the first $2\tau_b$ period and $4N_xH_zH_z \rightarrow 2N_yH_z$ in the second $2\tau_b$ period are avoided, while the $2N_yH_z \rightarrow N_x$ and

dx.doi.org/10.1021/ja107847d |J. Am. Chem. Soc. 2011, 133, 909–919

$N_x \rightarrow 2N_yH_z$ transfers are retained. For CH_3 groups, the choice of the corresponding delays is known to be important for accurate ^{13}C relaxation measurements.[29,30] $2N_yH_z$ and $8N_yH_zH_zH_z$ terms generated in the first $2\tau_b$ period are eliminated by a ^1H 90° $(-x)$ pulse and a subsequent gradient, retaining N_z during the delay T for the longitudinal relaxation measurement. The rest of the pulse sequence is the same as in the HISQC experiment.[3]

^{15}N Transverse Relaxation for NH_3^+ Groups. As is known for ^{13}C transverse relaxation for CH_3 groups, the ^{15}N transverse relaxation for NH_3^+ groups should be biexponential due to the strong effects of DD/DD cross correlation between two $^{15}N-^1H$ pairs. The biexponential relaxation effects are manifested through:

$$f(T) = (3/4)\exp(-R_{2,\mathrm{slow}}T) + (1/4)\exp(-R_{2,\mathrm{fast}}T) \quad (3)$$

with the relaxation rates given by:[21]

$$R_{2,\mathrm{slow}} \approx 2J_{\mathrm{auto}}(0) - (4/3)J_{\mathrm{NHNH}}(0) \quad (4)$$

$$R_{2,\mathrm{fast}} \approx 2J_{\mathrm{auto}}(0) + 4J_{\mathrm{NHNH}}(0) \quad (5)$$

In the energy level diagram of an AX_3 spin system, the $R_{2,\mathrm{slow}}$ rates are related to two ^{15}N transitions in the $I = 3/2$ manifold and four transitions in the $I = 1/2$ manifolds, whereas the $R_{2,\mathrm{fast}}$ rates are related to two transitions in the $I = 3/2$ manifold.[10,29]

Figure 2b shows the pulse sequence for the ^{15}N transverse relaxation measurement, in which the CW-CPMG scheme[31] is implemented for maintaining the in-phase single-quantum coherence N_+ and thereby effectively eliminating the scalar relaxation during the T period. Hansen et al. originally proposed the CW-CPMG scheme for the improvement of relaxation dispersion experiments of backbone ^{15}N nuclei,[31] and the scheme has recently been incorporated into the CPMG experiment for ^{13}C methyl groups as well.[32] This scheme contains two CPMG blocks[33,34] that sandwich a refocusing pulse, and the ^1H continuous wave (CW) is applied during each of CPMG blocks. The application of ^1H−CW makes the relaxation rates for the four ^{15}N transitions associated with the $I = 3/2$ manifold become equal, while the other four ^{15}N transitions in the $I = 1/2$ manifolds remain unaffected.[29] As a result, the overall relaxation effect during the T period is given by:

$$f(T) = (1/2)\exp(-R_{2,\mathrm{ave}}T) + (1/2)\exp(-R_{2,\mathrm{slow}}T) \quad (6)$$

for which the average ^{15}N relaxation rate $R_{2,\mathrm{ave}}$ for the $I = 3/2$ manifold is $(R_{2,\mathrm{slow}} + R_{2,\mathrm{fast}})/2$. The initial rate $R_{2,\mathrm{ini}}$ for the ^{15}N transverse relaxation is given by:

$$R_{2,\mathrm{ini}} = f'(0) = (3/4)R_{2,\mathrm{slow}} + (1/4)R_{2,\mathrm{fast}} \quad (7)$$

for both eqs 3 and 6. As evident from eqs 4, 5, and 7, $R_{2,\mathrm{ini}}$ is independent of the N−H/N−H cross correlation. It is a function of $J_{\mathrm{auto}}(\omega)$ according to:[15]

$$R_{2,\mathrm{ini}} = 2J_{\mathrm{auto}}(0) + (3/2)J_{\mathrm{auto}}(\omega_N) + 3J_{\mathrm{auto}}(\omega_H + \omega_N) + 3J_{\mathrm{auto}}(\omega_H) + (1/2)J_{\mathrm{auto}}(\omega_H - \omega_N) \quad (8)$$

Thus, the $R_{2,\mathrm{ini}}$ rates are useful for the analysis of the dynamics of the NH_3^+ groups. As shown in the Supporting Information, the biexponential decay (eq 6) and single-exponential decay according to $\exp(-R_{2,\mathrm{init}}T)$ are almost linear and virtually indistinguishable for the first 30% decay, for which the use of single-exponential fitting for determination of $R_{2,\mathrm{init}}$ is valid. Because of the intrinsically slow ^{15}N transverse relaxation of NH_3^+ groups, the validity range covers the entire range of practically available ^{15}N−CPMG lengths (<150 ms) in the present study (Supporting Information).

Heteronuclear NOE for NH_3^+ Groups. Although use of a train of ^1H 120° pulses has been common in heteronuclear NOE measurements, recent studies have shown that the use of a train of ^1H 120° pulses for ^1H saturation can cause errors in heteronuclear NOE measured for protein backbone amide groups.[35,36] Use of 180° pulses for the ^1H saturation period was demonstrated to be an effective remedy.[35,36] While the use of 180° pulses instead of 120° pulses is suitable for achieving an ideal steady state for ^{15}N longitudinal magnetizations of NH_3^+ groups as well, the way 180° pulses work for ideal steady state is quite different for NH_3^+ groups because the types of relevant cross correlation pathways present are different. When H_z is saturated (i.e., $\langle H_z\rangle = 0$) in the steady state, the behaviors of N_z and $4N_zH_zH_z$ terms are given by the following differential equations with cross correlation taken into account.[37]

$$\frac{d}{dt}(\langle N_z\rangle - N_\infty) = -R_1(\langle N_z\rangle - N_\infty) + \sigma_{\mathrm{NH}}(H^a_\infty + H^b_\infty + H^c_\infty) - \Gamma_{\mathrm{NHNH}}(\langle 4N_zH^a_zH^b_z\rangle + \langle 4N_zH^b_zH^c_z\rangle + \langle 4N_zH^c_zH^a_z\rangle) \quad (9)$$

$$\frac{d}{dt}\langle 4N_zH^a_zH^b_z\rangle = -R(4N_zH_zH_z)\langle 4N_zH^a_zH^b_z\rangle - \Gamma_{\mathrm{NHNH}}(\langle N_z\rangle - N_\infty) + \Gamma_{\mathrm{HHHN}}(H^a_\infty + H^b_\infty) \quad (10)$$

$$\frac{d}{dt}\langle 4N_zH^b_zH^c_z\rangle = -R(4N_zH_zH_z)\langle 4N_zH^b_zH^c_z\rangle - \Gamma_{\mathrm{NHNH}}(\langle N_z\rangle - N_\infty) + \Gamma_{\mathrm{HHHN}}(H^b_\infty + H^c_\infty) \quad (11)$$

$$\frac{d}{dt}\langle 4N_zH^c_zH^a_z\rangle = -R(4N_zH_zH_z)\langle 4N_zH^c_zH^a_z\rangle - \Gamma_{\mathrm{NHNH}}(\langle N_z\rangle - N_\infty) + \Gamma_{\mathrm{HHHN}}(H^c_\infty + H^a_\infty) \quad (12)$$

where H_∞ and N_∞ represent Boltzmann magnetizations; σ_{NH} is a heteronuclear cross relaxation rate; $R(4N_zH_zH_z)$ is an auto relaxation rate for a $4N_zH_zH_z$ term; Γ_{NHNH} is the N−H/N−H cross correlation for longitudinal relaxation; and Γ_{HHHN} is the H−H/H−N cross correlation within the AX_3 spin system for longitudinal relaxation. N−H/N−H cross correlation interconverts N_z and $4N_zH_zH_z$, whereas H−H/H−N cross correlation interconverts H_z and $4N_zH_zH_z$. The rates for cross relaxation and cross correlations are:[37]

$$\sigma_{\mathrm{NH}} = 2J_{\mathrm{auto}}(\omega_H + \omega_N) - (1/3)J_{\mathrm{auto}}(\omega_H - \omega_N) \quad (13)$$

$$\Gamma_{\mathrm{NHNH}} = 2J_{\mathrm{NHNH}}(\omega_N) \quad (14)$$

$$\Gamma_{\mathrm{HHHN}} = 2J_{\mathrm{HHHN}}(\omega_H) \quad (15)$$

Our pulse sequence for the heteronuclear NOE measurement is designed so that $\langle 4N_zH_zH_z\rangle$ terms are unperturbed by ^1H pulses in the ^1H saturation period, thereby providing a better steady state for ^{15}N longitudinal magnetization. The pulse

sequence for the heteronuclear NOE measurement is shown in Figure 2c. By using ^{1}H 180° pulses instead of 120° pulses, $\langle H_z \rangle$ is saturated without perturbing $\langle 4N_zH_zH_z \rangle$ in this pulse sequence. To compensate the pulse imperfection, 180° pulses along x and $-x$ are applied alternately in the saturation period. With this pulse sequence, the heteronuclear NOE is given by:

$$\mathrm{NOE} = 1 + 3\left(\frac{\gamma_H}{\gamma_N}\right)\frac{\sigma_{NH}R(4N_zH_zH_z) - 2\Gamma_{NHNH}\Gamma_{HHHN}}{R_1R(4N_zH_zH_z) - 3\Gamma^2_{NHNH}} \quad (16)$$

which is derived from eqs 9−12 with all time derivatives set to zero for the steady state. If the $R(4N_zH_zH_z)$ is much larger than the other rates involved in this equation, the heteronuclear NOE becomes:

$$\mathrm{NOE} = 1 + 3\left(\frac{\gamma_H}{\gamma_N}\right)\frac{\sigma_{NH}}{R_1} \quad (17)$$

which corresponds to the standard form for the case with no cross correlation involved.

Practically, the signal intensity for the reference spectrum in the heteronuclear NOE experiment is influenced by hydrogen exchange. If the recovery level of water magnetization is not 100%, the signal intensity for the reference spectrum can become weaker.[38−41] These effects can introduce substantial errors in the heteronuclear NOEs. In our heteronuclear NOE experiment, these problems were avoided by implementation of the water-flip-back scheme[38] and the use of a very long recycle delay (12 and 18 s at 600 and 800 MHz, respectively).

Relaxation of Longitudinal Three-Spin Order Term $4N_zH_zH_z$. While cross relaxation rate σ_{NH} and cross correlation rates Γ_{NHNH} and Γ_{HHHN} in eq 16 are a function of the correlation times and the order parameters under the assumption that the geometry of NH_3^+ groups is ideally tetrahedral, $R(4N_zH_zH_z)$ needs to be experimentally determined because it depends on other factors. The relaxation rate for $4N_zH_zH_z$ terms is given by:

$$R(4N_zH_zH_z) \approx R_1 + 2(\rho_{HH} + k_{ex}^{water}) \quad (18)$$

where R_1 is defined in eq 2; and ρ_{HH} is the rate of auto relaxation for a ^{1}H nucleus in the AX_3 system via dipole−dipole interactions with external ^{1}H nuclei.[3,42] As is demonstrated below, for an NH_3^+ group, the hydrogen exchange rate k_{ex}^{water} typically dominates in $R(4N_zH_zH_z)$. Figure 2d shows the pulse sequence for the measurement of $R(4N_zH_zH_z)$ for lysine NH_3^+ groups. In this pulse sequence, $4N_zH_zH_z$ terms are created at the beginning of the delay T, and the peak intensities are measured as a function of T. Although the $4N_zH_zH_z \rightarrow N_z$ transfer via N−H/N−H cross correlation during the delay T in this pulse sequence can contribute to the change of the intensity as a function of T, the effect can be neglected in good approximation, because Γ_{NHNH} is much smaller than $R(4N_zH_zH_z)$ for NH_3^+ groups.

Calculation of Order Parameters and Correlation Times for Internal Motions of NH_3^+ Groups. The measurements of ^{15}N R_1, ^{15}N $R_{2,ini}$, heteronuclear NOE, and $R(4N_zH_zH_z)$ permit the determination of the order parameter S^2_{axis} and correlation times τ_i and τ_f of internal motions for lysine NH_3^+ groups via nonlinear least-squares fitting based on eqs 1, 2, 8, and 13−16. During fitting, the following function that contains weighted squares for R_1, $R_{2,ini}$, and NOE is minimized:

$$\chi^2 = \sum \frac{(Y_{obs} - Y_{cal})^2}{Y^2_{obs}} \quad (19)$$

where Y_{obs} and Y_{cal} stand for observed and calculated quantities, respectively, of R_1, $R_{2,ini}$, and NOE. Because the overall molecular rotational correlation time τ_m can be accurately determined from the backbone ^{15}N relaxation data, the number of fitting parameters in the nonlinear least-squares fitting is three (i.e., S^2_{axis}, τ_f, and τ_i), which makes the use of relaxation data at multiple magnetic fields desirable.

MATERIALS AND METHODS

NMR Samples. Lyophilized powders of ^{15}N-labeled or ^{13}C/^{15}N-labeled ubiquitin were purchased from VLI research. The buffer of the protein solution was exchanged to 20 mM d_6-succinate·NaOH (pH 5.0), 40 mM NaCl, and 0.4 mM NaF (as an antimicrobial agent) by using Amicon Ultra-4 (Millipore). The powder of d_6-succinate was purchased from Sigma-Isotec. A 270 μL solution of 1 mM ubiquitin was sealed into an inner tube (diameter, 4.1 mm) of a 5 mm coaxial NMR tube system (Shigemi). No D_2O was used for the protein solution because the presence of the isotopomers NH_2D^+ and NHD_2^+ should be avoided for the analysis of NH_3^+ groups. The outer layer of the coaxial tube contained 100 μL of 100% d_4-methanol (Cambrdige Isotopes Laboratory) for NMR lock (100% D_2O could not be used because its freezing point is higher than the measurement temperature).

NMR Measurements. All NMR experiments were performed at 2 °C with Varian 800 and 600 MHz NMR spectrometers equipped with a noncryogenic HCN triple resonance probe. ^{13}C/^{15}N-labeled protein was used for the resonance assignment. Backbone and side-chain resonances were assigned by using three-dimensional HNCA, HN(CO)CA, HNCO, HN(CA)CO, HNCACB, CBCA(CO)NH, H(CCO)NH, C(CO)NH, HCCH−TOCSY, and HCCH−COSY spectra[43] measured at 2 °C. Lysine NH_3^+ groups were assigned with lysine-specific triple resonance experiments H_2CN, H_3NCECD, HDHE(CDCE)NH_3, and $CCENH_3$.[3,5,44]

The ^{15}N relaxation parameters for NH_3^+ groups were measured at ^{1}H frequencies of 600 and 800 MHz for the ^{15}N-labeled ubiquitin solution using the pulse sequences shown in Figure 2. Two-dimensional ^{1}H−^{15}N correlation spectra for the relaxation analyses were recorded typically with 100 and 512 complex points for the t_1 and t_2 periods, respectively. The spectral widths for the ^{15}N and ^{1}H dimensions were 4.4 and 15.9 ppm, respectively. Relaxation rates were measured with eight different lengths of the delay T: 40, 320, 600, 880, 1160, 1440, 1720, and 2000 ms for ^{15}N R_1 rates; 16, 33, 49, 66, 82, 98, 115, and 131 ms for ^{15}N $R_{2,ini}$; and 1, 3, 7, 13, 21, 31, 43, and 57 ms for $R(4N_zH_zH_z)$. The eight-point measurement of $R_{2,ini}$ was performed with a CPMG effective field strength ν_{CPMG} = 122 Hz. Because of the slow transverse relaxation of NH_3^+ groups, a relatively long time can be used for the constant-time relaxation dispersion experiment, which permits sensitive detection of slow dynamics. The CPMG relaxation dispersion experiment was carried out with a constant time CPMG period of 100 ms with 10 different ν_{CPMG} values ranging from 10 to 120 Hz. For the heteronuclear NOE measurements, it was found that the use of a long recycle delay (12 s at 600 MHz and 18 s at 800 MHz) was necessary for measurement accuracy. With a recycle delay much shorter than this, the intensities of the signals in the reference spectrum become significantly weaker due to incomplete recovery of water magnetization and the rapid hydrogen exchange, and, as a result, the absolute value of the heteronuclear NOE becomes substantially larger. More details of the relaxation measurements are given in the caption of Figure 2. The CLEANEX-HISQC experiment[3] were performed at 600 MHz ^{1}H frequency for the analysis of hydrogen exchange for the lysine NH_3^+ groups. The hydrogen exchange rates k_{ex}^{water} were calculated as described by Hwang et al.[45] For determination of the molecular rotational correlation time τ_m of ubiquitin at 2 °C, backbone ^{15}N R_1 and R_2 relaxation rates were also measured at 800 MHz

^{1}H frequency. The value of τ_m and the anisotropy of the axially symmetric rotational diffusion tensor were determined from the backbone R_1 and R_2 data as described previously.[27] NMR data were processed with NMRPipe[46] and analyzed with the NMRView[47] software.

Determination of Order Parameters and Internal Motion Correlation Times from NMR Data. ^{15}N relaxation rates R_1 and $R_{2,ini}$, heteronuclear NOE, and $R(4N_zH_zH_z)$ measured at 600 and 800 MHz proton frequencies were used for the calculation of order parameters S^2_{axis} and correlation times τ_i and τ_f. Minimization of χ^2 function of eq 19 was performed with the Mathematica 7 software (Wolfram). Based on neutron diffraction data,[18] $S^2_f = 0.111$ for $J_{auto}(\omega)$ and $J_{NHNH}(\omega)$, $S^2_f = 0.167$ for $J_{HHHN}(\omega)$, and $r_{NH} = 1.04$ Å were used in the calculations. Errors of the fitting parameters were estimated by a Monte Carlo approach. The Mathematica script and its output are given in the Supporting Information.

Analysis of Lysine NH_3^+ Groups in the Molecular Dynamics Simulation. Order parameters for the symmetry axes of lysine NH_3^+ groups (i.e., Cε−NζH$_3^+$ bonds) were calculated from a 1 μs molecular dynamics simulation at 300 K using the AMBER 9 software package[48] with the AMBER ff99SB force field,[49] which was shown to accurately reproduce protein dynamics. The trajectory used in this work was extended from the trajectory that had been used in a previous study.[50] The SHAKE algorithm[51] was employed to constrain all bonds involving hydrogen atoms, and a time step of 2 fs was used. The protein molecule was embedded in a cubic box with SPC/E water models,[52] and long-range electronic interactions were handled using the PME method[53] at a real space cutoff of 8 Å. The starting coordinates were taken from the 1.8 Å resolution crystal structure (PDB 1UBQ),[54] and the simulations were run for 1 μs after application of standard minimization and heating protocols. Autocorrelation functions for Cε−Nζ bonds of lysine residues in ubiquitin were obtained from the trajectory as described previously.[23] The order parameters for the Cε−Nζ bonds were calculated as the average plateau of the autocorrelation functions between 4−6 ns and by the iRED approach[55] with a time-window of 4 ns. Hydrogen bonds involving lysine NH_3^+ groups in the trajectory were analyzed with the PTRAJ program in the AMBER package.

RESULTS

Heteronuclear NMR of Lysine NH_3^+ Groups in Ubiquitin. Human ubiquitin contains seven lysine residues: Lys6, Lys11, Lys27, Lys29, Lys33, Lys48, and Lys63 (Figure 3a). At pH 5.0 and 2 °C, the ^{15}N-labeled ubiquitin exhibited six well-isolated signals from lysine amino groups in the HISQC spectrum (Figure 3b). The F1-^{1}H-coupled HSQC spectrum for lysine amino groups[3,4,13] clearly indicated that the spin systems for the observed amino groups are AX_3 rather than AX_2 (data not shown), and, therefore, these amino groups are protonated (i.e., NH_3^+ groups). Using the lysine-specific triple resonance spectra[3,5,44] as well as standard backbone and side-chain double/triple resonance spectra,[43] we unambiguously assigned the NH_3^+ signals as shown in Figure 3b. Under the current experimental conditions, Lys6 was not observed in the HISQC spectrum presumably due to faster hydrogen exchange with water. In fact, a previous study reported that Lys6 side-chain exhibits more than 5-fold faster hydrogen exchange rates than the other lysine side-chains in ubiquitin.[2] The signal from Lys27 NH_3^+ group is located at a unique position for which the ^{15}Nζ chemical shift is 34.2 ppm. The unique ^{15}N chemical shift of this group may be due to its two hydrogen bonds with Asp52 Oδ and Gln41 O found in the crystal structure.

^{15}N Relaxation for Lysine NH_3^+ Groups. Using the pulse sequences shown in Figure 2, we measured ^{15}N R_1, ^{15}N $R_{2,ini}$, heteronuclear ^{1}H−^{15}N NOE, and $R(4N_zH_zH_z)$ for lysine NH_3^+ groups at 800 and 600 MHz ^{1}H frequencies. Table 1 shows lysine side-chain ^{15}N R_1, ^{15}N $R_{2,ini}$ rates, whereas Table 2 shows heteronuclear ^{1}H−^{15}N NOE and $R(4N_zH_zH_z)$ parameters for lysine NH_3^+ groups. The hydrogen exchange rates k_{ex}^{water} measured at 600 MHz with CLEANEX-HISQC are also shown in Table 2. Examples of the relaxation data for the NH_3^+ groups of Lys27 and Lys48 are shown in Figure 4.

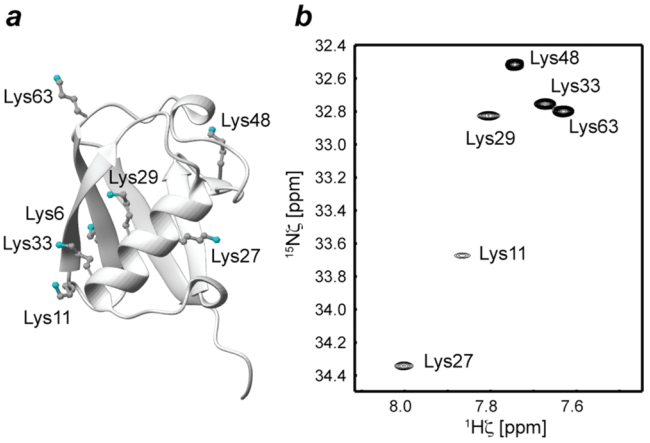

Figure 3. (a) Lysine side-chains in the crystal structures of human ubiquitin (PDB code: 1UBQ). Nζ atoms of the lysine NH_3^+ groups are shown in cyan. (b) The HISQC spectrum recorded on lysine NH_3^+ groups in ^{15}N-labeled human ubiquitin (1 mM) at pH 5.0 and 2 °C. For avoiding isotopically different species for NH_3^+ groups, no D_2O was used in the protein solution. The deuterium signal from d_4-methanol separately sealed in the outer layer of the coaxial NMR tube system was used for NMR lock. Signals from the NH_3^+ groups were assigned using lysine-specific triple resonance experiments (see text).

The most remarkable aspect of ^{15}N relaxation of NH_3^+ groups is their very slow transverse relaxation, for which the initial rates $R_{2,ini}$ range from 0.98 to 4.24 s^{-1} for ubiquitin at 2 °C. The ^{15}N $R_{2,ini}$ rates of lysine NH_3^+ groups are 6−12-fold slower than backbone ^{15}N R_2 of the same residues. Because of the small ^{15}N gyromagnetic ratio, ^{15}N $R_{2,ini}$ for NH_3^+ group is substantially smaller than ^{13}C $R_{2,ini}$ for a CH_3 group in the same environment. The slow $R_{2,ini}$ rates are responsible for very sharp ^{15}N lineshapes of HISQC signals as seen in Figure 3b.

Because the CW-CPMG scheme is suitable for relaxation dispersion experiments to study dynamics occurring on the microsecond−millisecond time scale,[31,32] we also measured $R_{2,ini}$ using different CPMG field strengths ν_{CPMG} for investigating the slow dynamics of the lysine side-chains. The $R_{2,ini}$ rate for the NH_3^+ groups of Lys27 was found to be faster when ν_{CPMG} is small (Figure 4c), while $R_{2,ini}$ rates were virtually independent of ν_{CPMG} for all the other lysine NH_3^+ groups. Provided that the slow dynamics observed for Lys27 NH_3^+ is a two-state exchange, the exchange rate for the process was calculated to be 93 ± 33 s^{-1} using expressions given by Loria et al.[56]

The ^{15}N R_1 rates for NH_3^+ groups were found to be between 0.4 and 1.8 s^{-1}. Field-dependence of the ^{15}N R_1 rates was stronger than that for $R_{2,ini}$; the ^{15}N R_1 rates at 800 MHz were 10−20% smaller than those at 600 MHz. As compared to the backbone ^{15}N R_1 rates for the same lysine residues (0.89−0.94 s^{-1} at 800 MHz), the ^{15}N R_1 rates for NH_3^+ groups display larger variation. The slowest NH_3^+ R_1 rates (Lys63) were only ∼2-fold slower than backbone ^{15}N R_1 of the same lysine residues.

As shown in Table 2, all values of the heteronuclear NOE measured for lysine NH_3^+ groups were negative and ranged

Table 1. ^{15}N R_1 and $R_{2,ini}$ Rates for Lysine NH_3^+ Groups in Human Ubiquitin[a]

	^{15}N R_1 [s^{-1}]		^{15}N $R_{2,ini}$ [s^{-1}]	
NH_3^+	800 MHz	600 MHz	800 MHz	600 MHz
Lys11	0.661 ± 0.010 (0.674)	0.776 ± 0.026 (0.770)	1.815 ± 0.089 (1.662)	1.629 ± 0.167 (1.724)
Lys27	1.431 ± 0.018 (1.595)	1.773 ± 0.035 (1.979)	4.237 ± 0.072 (3.348)	4.065 ± 0.132 (3.650)
Lys29	0.811 ± 0.003 (0.803)	0.933 ± 0.011 (0.948)	1.684 ± 0.034 (1.705)	1.852 ± 0.082 (1.816)
Lys33	0.419 ± 0.001 (0.421)	0.458 ± 0.002 (0.467)	0.971 ± 0.012 (1.005)	1.105 ± 0.024 (1.032)
Lys48	0.471 ± 0.001 (0.471)	0.504 ± 0.002 (0.512)	0.980 ± 0.010 (0.923)	0.915 ± 0.021 (0.949)
Lys63	0.404 ± 0.001 (0.416)	0.458 ± 0.003 (0.463)	1.130 ± 0.013 (1.046)	1.066 ± 0.026 (1.073)

[a] Values in parentheses are back-calculated relaxation rates as computed from the derived order parameters and correlation times.

Table 2. Heteronuclear (^1H) ^{15}N NOE, $R(4N_zH_zH_z)$ Rates, and Hydrogen Exchange Rates k_{ex}^{water} for Lysine NH_3^+ Groups in Human Ubiquitin[a]

	NOE		$R(4N_zH_zH_z)$ [s^{-1}]		
NH_3^+	800 MHz	600 MHz	800 MHz	600 MHz	k_{ex}^{water} [s^{-1}]
Lys11	−2.72 ± 0.09 (−2.87)	−2.92 ± 0.17 (−2.71)	147.1 ± 6.5	153.7 ± 17.3	71.0 ± 6.0
Lys27	−1.88 ± 0.05 (−1.94)	−2.38 ± 0.13 (−2.37)	59.2 ± 0.7	59.4 ± 1.4	18.7 ± 1.6
Lys29	−2.88 ± 0.05 (−2.91)	−3.01 ± 0.09 (−2.95)	103.1 ± 1.1	109.8 ± 2.8	43.1 ± 1.5
Lys33	−3.24 ± 0.03 (−3.28)	−3.18 ± 0.04 (−3.00)	42.5 ± 0.2	44.0 ± 0.2	17.6 ± 0.1
Lys48	−3.29 ± 0.02 (−3.45)	−3.54 ± 0.03 (−3.26)	18.1 ± 0.1	19.5 ± 0.1	8.8 ± 0.1
Lys63	−3.14 ± 0.02 (−3.24)	−3.30 ± 0.04 (−2.92)	40.8 ± 0.2	42.7 ± 0.2	17.1 ± 0.2

[a] Values in parentheses are back-calculated NOE as computed from the derived order parameters and correlation times.

from −3.54 to −1.88. Despite the use of the very long recycle delay, an ~3-day experiment with 48 scans per FID at 600 MHz (32 scans at 800 MHz) using a noncryogenic probe turned out to be sufficient to measure the heteronuclear NOE due to the slow decay during the t_1 evolution period. $R(4N_zH_zH_z)$ rates were found to be ~40−200-fold larger than R_1 for N_z and slightly larger than $2k_{ex}^{water}$ (Table 2). This indicates that the hydrogen exchange contribution dominates in eq 18. Although previous studies showed that lysine NH_3^+ groups forming hydrogen bonds with a ligand exhibited slower hydrogen exchange with water,[3,4] the present data suggest that the lysine NH_3^+ groups that do not form hydrogen bonds with other parts of the protein (i.e., Lys33, Lys48, and Lys63) exhibit slower hydrogen exchange rates and slower $R(4N_zH_zH_z)$ rates than those with hydrogen bonds (Lys11, Lys27, and Lys29). This might be because the hydrogen-bond acceptors could catalyze hydrogen exchange under particular conditions.[6] With the observed range of $R(4N_zH_zH_z)$ rates for lysine NH_3^+ groups, the use of eq 17 instead of eq 16 introduces only <3% error in heteronuclear NOE for the present case.

Order Parameters and Correlation Times for Internal Motions of Lysine NH_3^+ Groups. Using the experimental ^{15}N relaxation data and the spectral density model represented by eq 1, we determine the order parameters S^2_{axis}, and correlation times τ_f and τ_i for the internal motions of NH_3^+ groups. No exchange contributions to $R_{2,ini}$ were considered in the fitting procedure, because the CPMG relaxation dispersion data and the dependence of $R_{2,ini}$ on the magnetic field strength indicated absence of exchange contributions to the $R_{2,ini}$ rates. The resulting model-free parameters are shown in Table 3. The minimized χ^2 value for each NH_3^+ group is also shown.

The order parameters S^2_{axis} extracted for the lysine NH_3^+ groups in ubiquitin range from 0.192 to 0.709. The NH_3^+ groups of Lys11, Lys27, and Lys29, which form hydrogen bond(s) with other residues in the 1.8 Å resolution crystal structure, exhibit relatively large S^2_{axis} values (0.415, 0.709, and 0.378, respectively), suggesting that the hydrogen bonds restrict internal motions of NH_3^+ groups. In fact, the Lys27 side-chain that forms two hydrogen bonds has an order parameter larger than those of lysine side-chains that display a single hydrogen bond in the crystal structure.

Figure 5a shows a correlation between S^2_{axis} values for the NH_3^+ groups and isotropic crystallographic *B*-factors for corresponding Nζ atoms. Although the dynamic processes that determine crystallographic *B*-factors and NMR order parameters can differ,[57] a relatively strong anticorrelation with a correlation coefficient of −0.87 was observed between the two. Interestingly, a similar degree of correlation (correlation coefficient, −0.90) was found between the solvent accessible surface areas of Nζ atoms and the S^2_{axis} data for the NH_3^+ groups (Figure 5b). This result suggests that interactions with water, as opposed to interactions with other protein parts, pose a major effect on the mobility of the NH_3^+ groups. The S^2_{axis} order parameters predicted using a contact model originally developed for amino-acid methyl groups[58] also show a good correlation with respect to the experiment (correlation coefficient, 0.78).

The correlation times τ_f for NH_3^+ bond rotations were determined to be 24−29 ps for Lys33, Lys48, and Lys68, whereas the correlation times τ_i for reorientation of their symmetry axes were determined to be 100−128 ps. The bond rotations of the NH_3^+ groups that form a hydrogen bond with the other part of the protein were found to be slower than those of NH_3^+ groups with no hydrogen bonds. The bond rotation for Lys27 was found to be particularly slow with τ_f of 341 ps. The slow bond rotation of this residue may be due to two hydrogen bonds with other residues as suggested by the crystal structure. However, the spectral density model for this NH_3^+ group may not be as adequate as for the other NH_3^+ groups, because the value of the minimized χ^2 for Lys27 is significantly larger than those for the other lysine residues. The extracted values for τ_f for NH_3^+ bond rotations are comparable to those for CH_3 bond rotations, which are typically around 10−100 ps.[59−64] This may be somewhat surprising as one might expect that hydrogen bonds that can be formed with water molecules and other protein parts would make the rotations of NH_3^+ groups much slower than those of CH_3 groups. As discussed below, however, we find that the observed range of τ_f for NH_3^+ bond rotations is consistent with results obtained by alternative approaches.

Comparison with Order Parameters from the Molecular Dynamics Simulation. Because of recent improvements of molecular mechanics force fields and increased computer power for the simulation of longer and better-converged molecular

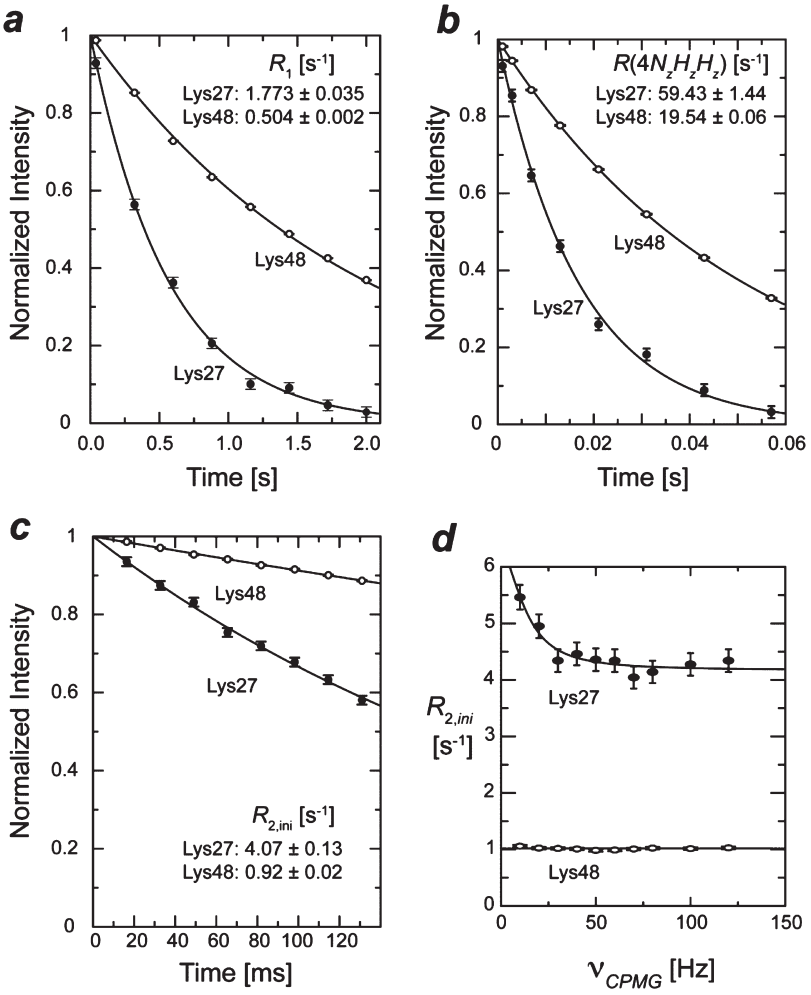

Figure 4. ^{15}N relaxation data for NH_3^+ groups of Lys27 and Lys48 at ^{1}H frequency of 600 MHz. (a) Relaxation of N_z measured with the pulse sequence shown in Figure 2a. (b) Relaxation of the longitudinal three-spin order term $4N_zH_zH_z$ measured with the pulse sequence shown in Figure 2d. (c) Transverse relaxation of the in-phase single quantum term N_y measured with the pulse sequence shown in Figure 2b. (d) Dependence of the initial transverse relaxation rate $R_{2,ini}$ on CPMG field strength ν_{CPMG}.

Table 3. Order Parameters S^2_{axis} and Correlation Times τ_f and τ_i for Lysine NH_3^+ Groups in Human Ubiquitin[a]

NH_3^+	S^2_{axis}[b]	τ_f [ps][c]	τ_i [ps][d]	χ^2_{min}[e]
Lys11	0.415 ± 0.039	38 ± 71	372 ± 207	0.0195
Lys27	0.709 ± 0.021	341 ± 11	0 ± 8	0.0822
Lys29	0.378 ± 0.017	199 ± 24	13 ± 66	0.0014
Lys33	0.248 ± 0.005	24 ± 1	114 ± 11	0.0095
Lys48	0.192 ± 0.005	29 ± 1	128 ± 8	0.0133
Lys63	0.267 ± 0.006	25 ± 1	100 ± 11	0.0179

[a] Fitting was carried out using the spectral density model of eq 1. A molecular rotational correlation time τ_m = 8.0 ns, which was determined from backbone ^{15}N R_1 and R_2 at 2 °C, was used for the calculation. The ideal tetrahedral geometry was assumed. [b] Order parameters for the symmetry axes. [c] Correlation times for bond rotations. [d] Correlation times for the internal reorientational motions of the symmetry axes. [e] Minimized values of the χ^2 function given by eq 19.

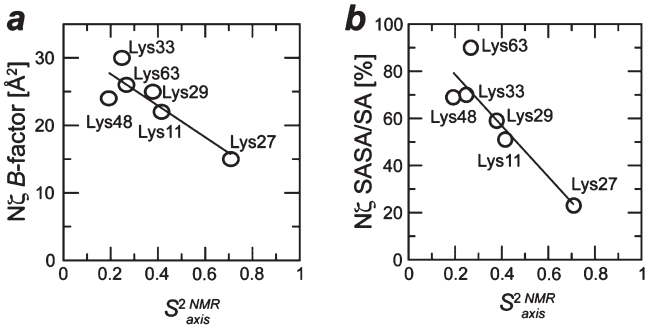

Figure 5. (a) Correlation between S^2_{axis} for lysine NH_3^+ groups and isotropic crystallographic *B*-factors for lysine Nζ atoms. (b) Correlation between S^2_{axis} for lysine NH_3^+ groups and solvent-accessible surface area (SASA). The vertical axis corresponds to the ratios of SASA to surface area (SA) for Nζ atoms. The 1.8 Å resolution crystal structure (PDB 1UBQ) was used for these plots.

dynamics (MD) calculations, semiquantitative to nearly quantitative agreement between MD-derived and experimental S^2 order parameters have been found for backbone amide,[49,65−67] side-chain methyl,[23] backbone Cα−Hα,[68] and arginine side-chain Nε−Hε[69] groups in proteins. We compared our experimental S^2_{axis} of NH_3^+ groups with those calculated from a 1 μs molecular dynamics simulation for human ubiquitin. Figure 6a shows the

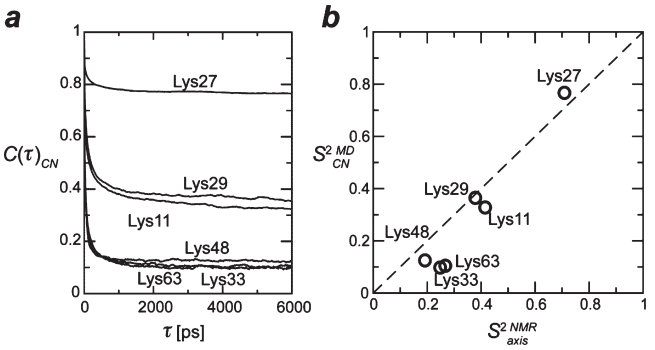

Figure 6. (a) Autocorrelation functions for lysine Cε−Nζ bond vectors calculated from the molecular dynamics simulation for ubiquitin. (b) Comparison of the experimental and computational order parameters S^2_{axis} for lysine NH_3^+ groups. The horizontal axis corresponds to the S^2_{axis} extracted from experimental NMR relaxation data on the lysine NH_3^+ groups, whereas the vertical axis corresponds to the order parameters calculated as the average between 4 and 6 ns of the autocorrelation functions for the Cε−Nζ bonds obtained from the molecular dynamics simulation.

autocorrelation functions for lysine Cε−Nζ bonds from the trajectory of the simulation. Because the bonds correspond to the symmetry axes of the lysine NH_3^+ groups, the plateaus of the autocorrelation functions in the displayed time window reflect the order parameters S^2_{axis}. As shown in Figure 6b, the order parameters from the NMR data agree reasonably well with those from the molecular dynamics simulation. The root-mean-square difference (rmsd) between them was 0.104. We also computed S^2_{axis} from the MD data by using the iRED approach with a time-window of 4 ns. The resulting values are systematically larger than those obtained from the autocorrelation functions by a small amount and agree slightly better with the experimental data (0.075 rmsd).

DISCUSSION

Bond Rotation and Hydrogen-Bonding Dynamics of Lysine NH_3^+ Groups. Until recently, experimental investigations of hydrogen-bond dynamics had been very difficult, even for small molecules. Recent experimental studies by vibrational spectroscopy together with ab initio molecular dynamics simulations have shown that the lifetime of a hydrogen bond between water molecules is ~1 ps.[70−72] Magnetic relaxation dispersion studies by Halle's group showed that the reorientation of water molecules in protein hydration layer is only 2-fold retarded as compared to bulk water.[73] Although NMR investigations of the hydrogen-bond scalar couplings have provided new insights into hydrogen bonds in proteins and nucleic acids (e.g., reviewed in ref 74), the current knowledge of the hydrogen-bonding dynamics for macromolecules is mainly based on macromolecular dynamics simulations. While modern molecular mechanics force fields of proteins used in molecular dynamics simulations have been improved by high-level ab initio quantum mechanical calculations, experimental validation of hydrogen-bond dynamics in macromolecules is clearly desirable. Our experimental data are suitable for validation, because the rotations of NH_3^+ groups should be accompanied by transient breakage of hydrogen bonds. Therefore, the average lifetime of a hydrogen bond in the molecular dynamics simulation involving a NH_3^+ group should be shorter than or comparable to the experimentally determined τ_f for the same NH_3^+ group.

Table 4. Hydrogen Bonds Involving Lysine NH_3^+ Groups Found in the Molecular Dynamics Simulation for Ubiquitin[a]

donor	acceptor	presence in 1UBQ[b]	occupancy[c]	average lifetime[d]
Lys11 Nζ	Glu34 Oε	yes	62%	20 ps
Lys27 Nζ	Asp52 Oδ	yes	72%	24 ps
Lys27 Nζ	Pro38 O	no	26%	15 ps
Lys29 Nζ	Glu16 O	yes	64%	31 ps
Lys29 Nζ	Asp21 Oδ	no	36%	60 ps
Lys33 Nζ	Thr14 O	no	41%	19 ps

[a] Only those with an occupancy higher than 25% are listed. [b] PDB coordinates of 1.8 Å crystal structure of ubiquitin. [c] Probability of the presence of a hydrogen bond in the MD trajectory. [d] Average lifetime of a hydrogen bond. Equivalent atoms (i.e., three hydrogen atoms in an NH_3^+ group and two oxygen atoms in a side-chain carboxyl group) were distinguished in the calculation of lifetimes, whereas they were not distinguished in the calculation of occupancies.

The NH_3^+ groups of Lys33, Lys48, and Lys63 do not form hydrogen bonds with other parts of the protein in the crystal structure. Their exposure to the solvent suggests that they can form hydrogen bonds with water molecules. A previous molecular dynamics study suggested that lifetimes of hydrogen bonds between a protein side-chain and water are 2−4 ps.[75] Our experimental data for the NH_3^+ groups of Lys33, Lys48, and Lys63 are consistent with the computational result, because obtained values of τ_f are longer than the suggested lifetimes of the water−side-chain hydrogen bonds.

The motions of the NH_3^+ groups of Lys11, Lys27, and Lys29 are restricted by hydrogen bond(s) with other protein parts. It is therefore not surprising that our experimental correlation times τ_f of these residues were longer than those for the other NH_3^+ groups with no hydrogen bonds, considering that the lifetimes of intramolecular hydrogen bonds are longer (15−60 ps) than lifetimes of hydrogen bonds between the protein and water molecules (2−4 ps) (see Table 4). This table lists intramolecular hydrogen bonds involving lysine NH_3^+ groups found in the molecular dynamics simulation. Their occupancies and average lifetimes in the trajectory are also shown. Some of them are not seen in the crystal structure, which is consistent with their occupancies in the trajectory well below 50%. The lifetimes of the intramolecular hydrogen bonds involving NH_3^+ groups are comparable to or shorter than the corresponding correlation times of the NH_3^+ bond rotations determined by NMR. Thus, both the molecular dynamics simulation and the NMR data suggest that hydrogen bonding by lysine NH_3^+ groups is highly dynamic with a subnanosecond lifetime.

Dynamics of the Functionally Important NH_3^+ Groups in Ubiquitin. The lysine NH_3^+ groups are critically important for the function of ubiquitin, because they are linkage sites for ubiquitination (or ubiquitylation) involved in various cellular processes such as protein degradation,[76] cell-cycle progression,[77] and immune responses.[78] The ubiquitin-conjugating enzyme E2 covalently attach ubiquitin to a target protein in the complex with the ubiquitin ligase E3. A lysine side-chain amino group of the target and the terminal carboxyl group of ubiquitin is linked in this process. The E2/E3 enzyme complex further extends the ubiquitin chain by linking a lysine side-chain NH_3^+ group of the conjugated ubiquitin to the terminal carboxyl group of the subsequent ubiquitin molecule. In this process, a polyubiquitin chain is formed, and its conformation depends on the linkage site.[79] The NH_3^+ group of Lys48 is the major linkage site, and the

Lys48-linked polyubiquitin chain is particularly important as a marker for proteasomal degradation.[76] Our NMR data indicate that the NH_3^+ group of precisely the same lysine is the most mobile amino group with an order parameter of 0.19. The NH_3^+ group of Lys63 is the second most abundant linkage site.[80] This NH_3^+ group is also highly mobile with an order parameter of 0.27. Interestingly, a recent proteomic study showed that the sequence biases and structural preferences around ubiquitination sites on target proteins are similar to those of intrinsically disordered protein regions,[81] which implicates that the lysine amino groups of the target proteins for the initial ubiquitination exhibit also a high degree of mobility. This property together with the solvent exposure of the substrate lysine NH_3^+ group might be key determinants for the efficiency of ubiquitination by the E2/E3 enzyme complex. While immobilization of the highly dynamic lysine side-chain by the ubiquitination process is obviously unfavorable in terms of entropy, it is difficult to estimate the actual free energy cost from a change of the NH_3^+ order parameter alone. This is because, even if a salt-bridge immobilizes the NH_3^+ group, CH_2 methylene groups of the same residue can still undergo substantial internal motions in a concerted way such that the side-chain end group is little affected, analogous to the situation encountered in arginine side-chains.[69] A quantitative assessment of the entropy changes of lysine side-chains would need to take into account also changes in the dynamics of CH_2 moieties.[69]

Potential Applications. The methods developed in this study can be applied to dynamics investigations of functionally important lysine side-chains in various cellular processes. For instance, applications to lysine side-chains at molecular interfaces of protein−DNA complexes and an lysine side-chain in the active site of an enzyme are underway in the laboratory of J.I. This methodology allows us to study dynamics of ion pairs and hydrogen bonds involving the lysine NH_3^+ groups. This methodology can also address effects of salt on NH_3^+ groups, which is important because modulation of ionic strength highly affects kinetics and thermodynamics of many macromolecular interactions, while atomic details about this phenomenon are unclear. Because of the very slow ^{15}N transverse relaxation of NH_3^+ groups, which is even slower than ^{13}C transverse relaxation of CH_3 groups, NH_3^+ groups can be used as alternative probes for the NMR investigations of large proteins or protein complexes, provided that hydrogen exchange is as slow as in the present case. In fact, Iwahara et al. demonstrated that the HISQC signals from lysine NH_3^+ groups in a 128 kDa protein were clearly observable at pH 5.5 and 10 °C.[3] While low pH and low temperature experimental conditions may compromise the biological relevance, observation of functionally important lysine amino groups at higher pH and temperature is still feasible because their hydrogen exchange processes tend to be slowed due to hydrogen bonding.[3,4,12] It should also be noted that there are many proteins for which low pH is biologically important, which include proteins in lysosome or vacuole cell organelles (pH is ~5)[82] and enzymes secreted in digestive organs.

CONCLUSIONS

In this work, we have established the methodology for the investigations of the dynamics of lysine NH_3^+ groups in proteins. The NMR methods provide the order parameters and correlation times for bond rotations and reorientations of symmetry axes occurring on a picosecond−nanosecond time scale as well as information about slower dynamics for NH_3^+ groups. The order parameters determined for lysine NH_3^+ groups in human ubiquitin were consistent with those from the molecular dynamics simulation. Interestingly, the lysine NH_3^+ groups crucial to ubiquitin's function were found to be highly mobile. This work has also provided important insights into the hydrogen-bond dynamics involving lysine NH_3^+ groups. The correlation times for the NH_3^+ bond rotations from the NMR experiment and the lifetimes of hydrogen bonds from the molecular dynamics simulation suggest that the formation and breakage of hydrogen bonds by lysine NH_3^+ groups occur on a subnanosecond time scale. Considering that relaxation of ^{15}N in-phase single quantum transverse magnetization of lysine NH_3^+ groups is remarkably slow, the NMR methods presented here are likely to be beneficial for studying lysine side-chains of larger proteins and their complexes.

ASSOCIATED CONTENT

Supporting Information. Validation of single-exponential fitting for determination of $R_{2,ini}$ rates; and Mathematica notebook inputs and outputs for the calculation of order parameters and correlation times for internal motions of lysine NH_3^+ groups from NMR relaxation data. This material is available free of charge via the Internet at http://pubs.acs.org.

AUTHOR INFORMATION

Corresponding Author
j.iwahara@utmb.edu

ACKNOWLEDGMENT

We thank Dr. Lewis Kay for providing us with a CW-CPMG pulse program for backbone amide ^{15}N, which was very helpful in developing the pulse sequence in Figure 2b. This work was supported by Grant MCB-0918362 from the National Science Foundation (to R.B.), Grant 49968-DNI4 from the American Chemical Society Petroleum Research Funds (to J.I.), and Grant H-1683 from the Welch Foundation (to J.I.). NMR facilities of the UTMB Sealy Center for Structural Biology and Molecular Biophysics were supported in part by the Sealy and Smith Foundation, the W. M. Keck Foundation, and the John S. Dunn Foundation.

REFERENCES

(1) Liepinsh, E.; Otting, G. *Magn. Reson. Med.* **1996,** *35*, 30–42.
(2) Segawa, T.; Kateb, F.; Duma, L.; Bodenhausen, G.; Pelupessy, P. *ChemBioChem* **2008,** *9*, 537–42.
(3) Iwahara, J.; Jung, Y. S.; Clore, G. M. *J. Am. Chem. Soc.* **2007,** *129*, 2971–80.
(4) Poon, D. K.; Schubert, M.; Au, J.; Okon, M.; Withers, S. G.; McIntosh, L. P. *J. Am. Chem. Soc.* **2006,** *128*, 15388–9.
(5) Takayama, Y.; Castañeda, C. A.; Chimenti, M.; García-Moreno, B.; Iwahara, J. *J. Am. Chem. Soc.* **2008,** *130*, 6714–5.
(6) Englander, S. W.; Downer, N. W.; Teitelbaum, H. *Annu. Rev. Biochem.* **1972,** *41*, 903–24.
(7) Bodenhausen, G.; Ruben, D. J. *Chem. Phys. Lett.* **1980,** *69*, 185–189.
(8) Bax, A.; Griffey, R. H.; Hawkins, B. L. *J. Magn. Reson.* **1983,** *55*, 301–315.
(9) Müller, L. *J. Am. Chem. Soc.* **1979,** *101*, 4481–4484.
(10) Ollerenshaw, J. E.; Tugarinov, V.; Kay, L. E. *Magn. Reson. Chem.* **2003,** *41*, 843–852.
(11) Tugarinov, V.; Hwang, P. M.; Ollerenshaw, J. E.; Kay, L. E. *J. Am. Chem. Soc.* **2003,** *125*, 10420–8.

(12) Blaum, B. S.; Deakin, J. A.; Johansson, C. M.; Herbert, A. P.; Barlow, P. N.; Lyon, M.; Uhrin, D. *J. Am. Chem. Soc.* **2010,** *132,* 6374–81.
(13) Takayama, Y.; Sahu, D.; Iwahara, J. *J. Magn. Reson.* **2008,** *194,* 313–6.
(14) Tomlinson, J. H.; Ullah, S.; Hansen, P. E.; Williamson, M. P. *J. Am. Chem. Soc.* **2009,** *131,* 4674–84.
(15) Abragam, A. *The Principle of Nuclear Magnetism*; Carendon Press: Oxford, 1961; pp 264−353.
(16) Sheppard, D.; Sprangers, R.; Tugarinov, V. *Prog. Nucl. Magn. Reson. Spectrosc.* **2010,** *56,* 1–45.
(17) Sarkar, S. K.; Hiyama, Y.; Niu, C. H.; Young, P. E.; Gerig, J. T.; Torchia, D. A. *Biochemistry* **1987,** *26,* 6793–800.
(18) Lehmann, M. S.; Koetzle, T. F.; Hamilton, W. C. *J. Am. Chem. Soc.* **1971,** *94,* 2657–2660.
(19) Wei, A.; Raymond, M. K.; Roberts, J. D. *J. Am. Chem. Soc.* **1997,** *119,* 2915–2920.
(20) Burke, T. E. *J. Magn. Reson.* **1970,** *2,* 120–140.
(21) Kay, L. E.; Torchia, D. A. *J. Magn. Reson.* **1991,** *95,* 536–547.
(22) Lipari, G.; Szabo, A. *J. Am. Chem. Soc.* **1982,** *104,* 4546–4559.
(23) Showalter, S. A.; Johnson, E.; Rance, M.; Brüschweiler, R. *J. Am. Chem. Soc.* **2007,** *129,* 14146–14147.
(24) Brüschweiler, R.; Liao, X.; Wright, P. E. *Science* **1995,** *268,* 886–9.
(25) Fushman, D.; Cowburn, D. *J. Biomol. NMR* **1999,** *13,* 139–47.
(26) Lee, L. K.; Rance, M.; Chazin, W. J.; Palmer, A. G., III. *J. Biomol. NMR* **1997,** *9,* 287–98.
(27) Tjandra, N.; Feller, S. E.; Pastor, R. W.; Bax, A. *J. Am. Chem. Soc.* **1995,** *117,* 12562–12566.
(28) Woessner, D. E. *J. Chem. Phys.* **1962,** *37,* 647–654.
(29) Kay, L. E.; Bull, T. E.; Nicholson, L. K.; Griesinger, C.; Schwalbe, H.; Bax, A.; Torchia, D. A. *J. Magn. Reson.* **1992,** *100,* 538–558.
(30) Palmer, A. G.; Wright, P. E.; Rance, M. *Chem. Phys. Lett.* **1991,** *185,* 41–46.
(31) Hansen, D. F.; Vallurupalli, P.; Kay, L. E. *J. Phys. Chem. B* **2008,** *112,* 5898–904.
(32) Baldwin, A. J.; Hansen, D. F.; Vallurupalli, P.; Kay, L. E. *J. Am. Chem. Soc.* **2009,** *131,* 11939–48.
(33) Carr, H. Y.; Purcell, E. M. *Phys. Rev.* **1954,** *94,* 630–638.
(34) Meiboom, S.; Gill, D. *Rev. Sci. Instrum.* **1958,** *29,* 688–691.
(35) Ferrage, F.; Cowburn, D.; Ghose, R. *J. Am. Chem. Soc.* **2009,** *131,* 6048–9.
(36) Ferrage, F.; Piserchio, A.; Cowburn, D.; Ghose, R. *J. Magn. Reson.* **2008,** *192,* 302–13.
(37) Kumar, A.; Grace, R. C. R.; Madhu, P. K. *Prog. Nucl. Magn. Reson. Spectrosc.* **2000,** *37,* 191–319.
(38) Grzesiek, S.; Bax, A. *J. Am. Chem. Soc.* **1993,** *115,* 12593–12594.
(39) Idiyatullin, D.; Daragan, V. A.; Mayo, K. H. *J. Magn. Reson.* **2001,** *153,* 138–143.
(40) Li, Y. C.; Montelione, G. T. *J. Magn. Reson., Ser. B* **1994,** *105,* 45–51.
(41) Skelton, N. J.; Palmer, A. G.; Akke, M.; Kordel, J.; Rance, M.; Chazin, W. J. *J. Magn. Reson., Ser. B* **1993,** *102,* 253–264.
(42) Skrynnikov, N. R.; Ernst, R. R. *J. Magn. Reson.* **1999,** *137,* 276–80.
(43) Cavanagh, J.; Fairbrother, W. J.; Palmer, A. G., III; Rance, M.; Skelton, N. J. *Protein NMR Sprectroscopy: Principles and Practice,* 2nd ed.; Elsevier Academic Press: Burlington, 2007.
(44) Andre, I.; Linse, S.; Mulder, F. A. *J. Am. Chem. Soc.* **2007,** *129,* 15805–13.
(45) Hwang, T. L.; van Zijl, P. C.; Mori, S. *J. Biomol. NMR* **1998,** *11,* 221–6.
(46) Delaglio, F.; Grzesiek, S.; Vuister, G. W.; Zhu, G.; Pfeifer, J.; Bax, A. *J. Biomol. NMR* **1995,** *6,* 277–293.
(47) Johnson, B. A.; Blevins, R. A. *J. Biomol. NMR* **1994,** *4,* 603–614.
(48) Case, D. A.; Cheatham, T. E., III; Darden, T.; Gohlke, H.; Luo, R.; Merz, K. M., Jr.; Onufriev, A.; Simmerling, C.; Wang, B.; Woods, R. J. *J. Comput. Chem.* **2005,** *26,* 1668–88.
(49) Hornak, V.; Abel, R.; Okur, A.; Strockbine, B.; Roitberg, A.; Simmerling, C. *Proteins* **2006,** *65,* 712–25.
(50) Li, D. W.; Brüschweiler, R. *J. Am. Chem. Soc.* **2009,** *131,* 7226–7.
(51) Ryckaert, J. P.; Ciccotti, G.; Berendsen, H. J. C. *J. Comput. Phys.* **1977,** *23,* 327–341.
(52) Berendsen, H. J. C.; Grigera, J. R.; Straatsma, T. P. *J. Phys. Chem.* **1987,** *91,* 6269–6271.
(53) Darden, T.; York, D.; Pedersen, L. *J. Chem. Phys.* **1993,** *98,* 10089–10092.
(54) Vijay-Kumar, S.; Bugg, C. E.; Cook, W. J. *J. Mol. Biol.* **1987,** *194,* 531–44.
(55) Prompers, J. J.; Bruschweiler, R. *J. Am. Chem. Soc.* **2002,** *124,* 4522–34.
(56) Loria, J. P.; Rance, M.; Palmer, A. G. *J. Am. Chem. Soc.* **1999,** *121,* 2331–2332.
(57) Brüschweiler, R.; Wright, P. E. *J. Am. Chem. Soc.* **1994,** *116,* 8426–8427.
(58) Ming, D.; Brüschweiler, R. *J. Biomol. NMR* **2004,** *29,* 363–8.
(59) Batchelder, L. S.; Sullivan, C. E.; Jelinski, L. W.; Torchia, D. A. *Proc. Natl. Acad. Sci. U.S.A.* **1982,** *79,* 386–9.
(60) Ishima, R.; Petkova, A. P.; Louis, J. M.; Torchia, D. A. *J. Am. Chem. Soc.* **2001,** *123,* 6164–71.
(61) Muhandiram, D. R.; Yamazaki, T.; Sykes, B. D.; Kay, L. E. *J. Am. Chem. Soc.* **1995,** *117,* 11536–11544.
(62) Nicholson, L. K.; Kay, L. E.; Baldisseri, D. M.; Arango, J.; Young, P. E.; Bax, A.; Torchia, D. A. *Biochemistry* **1992,** *31,* 5253–63.
(63) Xue, Y.; Pavlova, M. S.; Ryabov, Y. E.; Reif, B.; Skrynnikov, N. R. *J. Am. Chem. Soc.* **2007,** *129,* 6827–38.
(64) Zhang, X.; Sui, X.; Yang, D. *J. Am. Chem. Soc.* **2006,** *128,* 5073–81.
(65) Showalter, S. A.; Brüschweiler, R. *J. Chem. Theory Comput.* **2007,** *3,* 961–975.
(66) Soares, T. A.; Daura, X.; Oostenbrink, C.; Smith, L. J.; van Gunsteren, W. F. *J. Biomol. NMR* **2004,** *30,* 407–422.
(67) Trbovic, N.; Kim, B.; Friesner, R. A.; Palmer, A. G., III. *Proteins* **2008,** *71,* 684–94.
(68) Sheppard, D.; Li, D. W.; Godoy-Ruiz, R.; Brüschweiler, R.; Tugarinov, V. *J. Am. Chem. Soc.* **2010,** *132,* 7709–19.
(69) Trbovic, N.; Cho, J. H.; Abel, R.; Friesner, R. A.; Rance, M.; Palmer, A. G., III. *J. Am. Chem. Soc.* **2009,** *131,* 615–22.
(70) Gale, G. M.; Gallot, G.; Hache, F.; Lascoux, N.; Bratos, S.; Leicknam, J. C. *Phys. Rev. Lett.* **1999,** *82,* 1068–1071.
(71) Keutsch, F. N.; Saykally, R. J. *Proc. Natl. Acad. Sci. U.S.A.* **2001,** *98,* 10533–40.
(72) Lawrence, C. P.; Skinner, J. L. *Chem. Phys. Lett.* **2003,** *369,* 472–477.
(73) Halle, B. *Philos. Trans. R. Soc., B* **2004,** *359,* 1207–23.
(74) Grzesiek, S.; Cordier, F.; Jaravine, V.; Barfield, M. *Prog. Nucl. Magn. Reson. Spectrosc.* **2004,** *45,* 275–300.
(75) Bandyopadhyay, S.; Chakraborty, S.; Bagchi, B. *J. Am. Chem. Soc.* **2005,** *127,* 16660–7.
(76) Hershko, A.; Ciechanover, A. *Annu. Rev. Biochem.* **1992,** *61,* 761–807.
(77) Hershko, A. *Curr. Opin. Cell Biol.* **1997,** *9,* 788–99.
(78) Bhoj, V. G.; Chen, Z. J. *Nature* **2009,** *458,* 430–7.
(79) Fushman, D.; Walker, O. *J. Mol. Biol.* **2010,** *395,* 803–14.
(80) Peng, J.; Schwartz, D.; Elias, J. E.; Thoreen, C. C.; Cheng, D.; Marsischky, G.; Roelofs, J.; Finley, D.; Gygi, S. P. *Nat. Biotechnol.* **2003,** *21,* 921–6.
(81) Radivojac, P.; Vacic, V.; Haynes, C.; Cocklin, R. R.; Mohan, A.; Heyen, J. W.; Goebl, M. G.; Iakoucheva, L. M. *Proteins* **2010,** *78,* 365–380.
(82) Voet, D.; Voet, J. G. *Biochemistry,* 3rd ed.; Wiley: Hoboken, 2004.
(83) Shaka, A. J.; Keeler, J.; Freeman, R. *J. Magn. Reson.* **1983,** *53,* 313–340.
(84) Kupče, E.; Boyd, J.; Campbell, I. D. *J. Magn. Reson., Ser. B* **1995,** *106,* 300–303.
(85) Kay, L. E.; Xu, G. Y.; Yamazaki, T. *J. Magn. Reson., Ser. A* **1994,** *109,* 129–133.
(86) Hansen, D. F.; Kay, L. E. *J. Biomol. NMR* **2007,** *37,* 245–55.